Applied Physics B (2019) 125:1
https://doi.org/10.1007/s00340-018-7110-y

Applied Physics B
Lasers and Optics

Ag_2S quantum dots in the fields of picosecond and femtosecond UV and IR pulses: optical limiting, nonlinear absorption and refraction properties

Yue Fu[1,2] · Rashid A. Ganeev[1] · Chen Zhao[1,2] · Konda Srinivasa Rao[1] · Sandeep Kumar Maurya[1] · Weili Yu[1] · Ke Zhang[1,2] · Chunlei Guo[1,3]

Received: 21 August 2018 / Accepted: 26 November 2018 / Published online: 30 November 2018

Abstract
We demonstrate strong optical nonlinearities of silver sulfide (Ag_2S) quantum dots (QDs) in the ultraviolet range. The 4-nm Ag_2S QDs were prepared by chemical method and analyzed using picosecond (800 nm and 400 nm, 200 ps) and femtosecond (800 nm and 400 nm, 60 fs) laser pulses. Our Z-scan measurements show that these QDs have large nonlinear absorption coefficient (~ 10^{-3} cm W^{-1}) at 400 nm. We also demonstrate the transient absorption and optical limiting in Ag_2S QDs. Variations of the signs of nonlinear refractive indices and nonlinear absorption coefficients of QDs are demonstrated by changing pulse width and wavelength of probe radiation.

1 Introduction

Silver sulfide (Ag_2S) is an attractive low band gap ($E_g = 0.9$ eV) semiconductor material. Due to its excellent optical and electronic properties Ag_2S has promising applications as a material with large nonlinear optical (NLO) coefficients. The rapid development of such NLO materials, they still cannot meet the requirements for practical applications. One possible way to improve the NLO response of materials is to modify their structure [1, 2]. Alongside the unique NLO properties of nanoparticles and nanostructures there is a continuously growing interest induced by the influence of the size and shape of these nanoparticles. Moreover, the existence of surface plasmon resonance (SPR) in nanoparticles has always been useful for the realization of strong NLO response upon interaction with intense laser pulses.

With the advent of laser pulses in femtosecond time domain the need in materials which offer effective protection from lasers of certain wavelengths in different power regimes became significant. Among various materials semiconductor nanoparticles have excellent and interesting applications in optics, and particularly in optical limiting (OL). For this reason, any new synthesized semiconductor nanoparticles or quantum dots (QDs) require to be examined under different conditions using laser pulses of variable energies, wavelengths and durations to understand the NLO mechanisms and distinguish their attractive properties for practical applications [3–7]. In many semiconductor nanoparticles the decrease of their sizes can provide a way to tune their physical properties and observe new phenomena. In particular, colloidal semiconductor nanocrystals provide strong size-related optical and optoelectronic properties. These properties have been investigated for applications in solar cells [5], light-emitting diodes [6, 8], thin-film transistors [9–11], and biological imaging [12, 13].

The QDs-containing materials, particularly sulfide-based QDs, were given special attention due to their large low-order optical nonlinearities [14–16]. Particularly, various NLO processes can be induced in the ZnS nanoparticles which are useful in photonics [17–20]. The coexistence of reverse saturable absorption (RSA) and two-photon

✉ Rashid A. Ganeev
rashid@ciomp.ac.cn

Chunlei Guo
guo@optics.rochester.edu

[1] The Guo China-US Photonics Laboratory, State Key Laboratory of Applied Optics, Changchun Institute of Optics, Fine Mechanics and Physics, Chinese Academy of Sciences, Changchun 130033, China

[2] University of Chinese Academy of Sciences, Beijing 100039, China

[3] The Institute of Optics, University of Rochester, Rochester, NY 14627, USA

absorption (2PA) in silver sulfide suggests that Ag_2S QDs could be a very promising nonlinear medium for photonic devices in different time scales if these semiconductor nanocrystallites are incorporated in appropriate media, which retain the attractive features of both components. The Ag_2S QDs also demonstrate low-threshold optical limiting in the visible and near-IR ranges [21–24]. With low-power CW laser irradiation at 532 nm the large thermo-optic coefficient and nonlinear refractive index (γ) up to -1.5×10^{-7} $cm^2\ W^{-1}$ in the Ag_2S samples were reported [25]. The nonlinear absorption coefficients (β) in the case of Ag_2S QDs dispersed in gelatin and thioglycolic acid were measured to be 7×10^{-11} and 8×10^{-11} cm W^{-1} using 532 nm pulses [16]. Similar nonlinear optical absorption of the Ag_2S QDs pumped by 532-nm nanosecond laser pulses ($\beta=1.2\times10^{-12}$ cm W^{-1}) was reported in Ref. [16].

QDs may show variable NLO properties at different pulse durations and wavelengths. When QDs were pumped by nanosecond laser at 532 nm wavelength, most of measurements have shown the RSA [26]. However, when nanoparticles are excited by pico- and femtosecond laser pulses at wavelengths of 800 and 1064 nm, they can exhibit self-focusing effects, as well as negative and positive nonlinear absorption [26–30]. Notice that in most of previous studies of silver sulfide nanoparticles the optical nonlinearities were analyzed at the wavelengths of 532 and 1064 nm. Meanwhile, there is a shortage of the studies devoted to the analysis of the NLO properties of the Ag_2S QDs at wavelengths of Ti:sapphire femtosecond and picosecond laser and its second harmonic (800 and 400 nm).

A search for new applications of QDs is an important task for optical community. The interesting idea is to find the optimal conditions in application of such QDs as effective emitters of the high-order harmonics of femtosecond pulses for development of efficient source of coherent extreme ultraviolet radiation. To date a large number of experiments with gas clusters and nanoparticles as well as ablated nanoparticles was conducted. Qualitative assessments show that the application of a group of particles containing a few 1000 atoms is the most optimal for the maximum increase in the number of generated harmonic photons. The knowledge of the nonlinear absorptive and refractive properties of those small-sized structures will allow definition of the optimal conditions of excitation of the QDs for high-order harmonic generation during formation of plasma plumes containing such species.

In this paper, we demonstrate large nonlinear absorption ($\beta\approx10^{-3}$ cm W^{-1}) of silver sulfide quantum dots at $\lambda=400$ nm. We report the NLO properties of 4 nm Ag_2S QDs, which had been synthesized by a chemical method. These properties were measured using pulses of different wavelength and duration. We analyze the transient absorption and optical limiting in Ag_2S QDs. Variations of the sign of nonlinear refractive indices and nonlinear absorption coefficients of QDs are demonstrated by changing pulse width and wavelength of probe radiation. We show that these QDs have strong nonlinear absorption at 400 nm, which can be attributed to RSA. The large RSA can indirectly indicate the possibility of some transitions to be involved in the growth of nonlinear susceptibility. This process can particularly lead to enhancement of single harmonic or group of harmonics during frequency conversion of ultrashort laser pulses interacting with such QDs.

2 Experimental arrangements

2.1 Preparation and characterization of the Ag_2S quantum dots

The experimental procedure performed for the synthesis of silver sulfide quantum dots was adapted from the one described in Ref. [31]. The one-pot method was used for producing Ag_2S QDs. We added 72 mg of sulfur powder into the flask during the heating procedure by continuous stirring at 200 RPM until sulfur powder became completely dissolved. When temperature increased up to 197 °C, 4 mL of Ag-TOP (TOP for trioctylphosphine) was quickly injected, and then the reaction was allowed to proceed for 7 min at 167 °C. 20 mL of butanol was added to prevent solidification of the reaction mixture as it was cooled.

The QDs were twice cleaned by methyl alcohol in the centrifugal machine. To avoid the effect of too high concentration for the linear absorption measurements, we diluted the prepared QDs in water to make the samples containing different volume parts of QDs. The Ag_2S QDs of higher (0.375 mg mL^{-1}) and lower (0.125 mg mL^{-1}) concentrations, which correspond to 1.5×10^{-3} and 5×10^{-4} mol L^{-1} concentrations, were synthesized and marked as S1 and S2, respectively.

The synthesized samples were characterized by transmission electron microscopy (TEM) (JEM 2100F, JEOL) and absorption spectroscopy (Agilent Technologies). TEM analysis provided information about size distribution (see inset in Fig. 1b) and morphology of the synthesized QDs (Fig. 1a). It is seen from Fig. 1b that QDs of different sizes with a narrow distribution are present in the synthesized samples. The calculated average size of the QDs was about 4 nm.

Figure 1b shows the absorption spectra of S1 and S2 samples. The absorption curves were similar to each other with the corresponding band gaps (E_g) of these two samples defined to be 3 eV ($\lambda\approx410$ nm). These absorption spectra represented a superposition of absorption spectra of the QDs of different sizes. The small nanocrystal QDs (2–5 nm) showed a blue shift in the absorption edge that

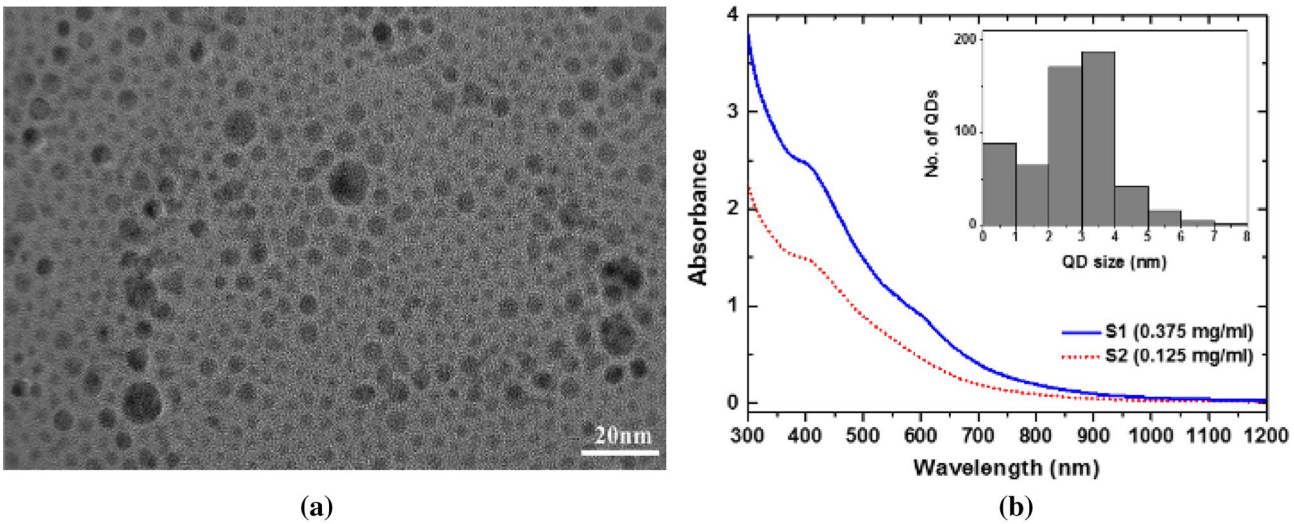

Fig. 1 **a** TEM image of Ag_2S QDs. **b** Absorption spectra of the S1 and S2 samples inserted in the 10-mm-thick cells. Inset: histogram of Ag_2S QDs size distribution

led to the change of effective band gap compared with the value ($E_g = 0.9$ eV) for bulk Ag_2S. The much larger band gap should cause a change of the refractive index and nonlinear absorption of this material [15]. Notice also the presence of small band at ~600 nm in the case of S1 sample.

2.2 Z-scan and pump–probe schemes

The standard Z-scan scheme [25] is a convenient method to measure the NLO parameters of materials. Our Ti:sapphire laser (Spitfire Ace, Spectra-Physics) provided 60 fs, 800 nm and 200 ps, 800 nm pulses at 1 kHz pulse repetition rate. We also used the second harmonic of this radiation ($\lambda = 400$ nm) to analyze NLO properties in the vicinity of the SPR. This radiation was focused by a 400-mm focal length spherical lens and measured using a large area photodetector (Fig. 2a).

Open-aperture (OA) scheme with fully opened aperture placed in front of photodetector allowed measurement of the nonlinear absorption of the Ag_2S QD suspensions in the 2-mm-thick fused silica cells during their propagation through the focal plane. In the case of closed-aperture (CA) Z-scan the 1-mm aperture allowed propagation of ~10% of output radiation. These measurements of propagated radiation led to determination of the nonlinear refraction of our samples. The CA scheme allowed calculation of the sign and magnitude of γ and β of QD-containing medium. The OA Z-scan was used for the measurements of β, which were compared with the measurements of this parameter using the CA scheme.

The analysis of Z-scan traces is based on the assumption that laser radiation has a Gaussian beam profile. Hence, prior to Z-scan measurements, we characterized the probe beam using a CCD camera (Thorlabs) and confirmed that

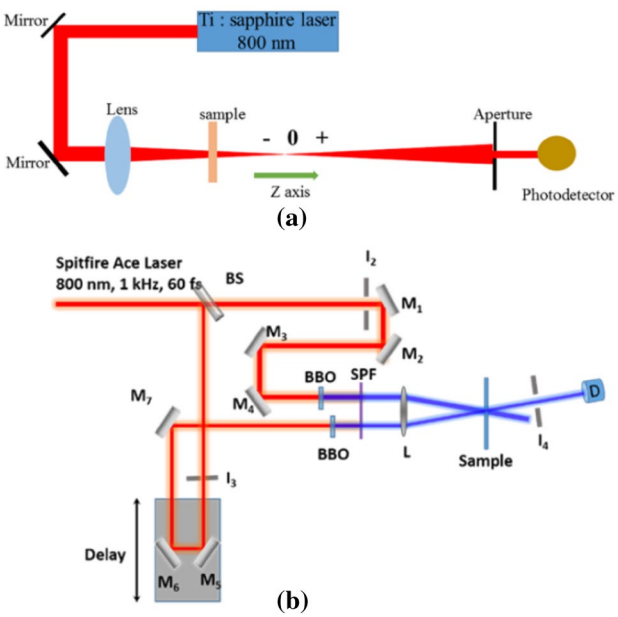

Fig. 2 **a** Z-scan scheme. **b** Schematic of transient absorption experiments. *BS* beam splitter, *M* mirrors, *L* lens, *f* 300 mm, *I* iris apertures, *BBO* barium borate crystals, *D* detector, *SPF* short-pass filter, *S* sample

the beam profile in the focal area was close to Gaussian, which is a prerequisite for the analysis of Z-scan traces using the relations developed for this technique. The full widths of focused femtosecond and picosecond beams at $1/e^2$ level of intensity distribution were measured to be 72 μm and 38 μm after focusing by 400- and 200-mm focal length lenses. Similar scheme was also used for OL studies.

The noncollinear pump–probe technique was employed to analyze transient absorption (TA) in the Ag_2S QDs using 400-nm radiation. Schematic of our experimental setup is shown in Fig. 2b. The 800-nm radiation was split by a beam splitter at the ratio of 30:70. The transmitted beam was used as a pump pulse and the reflected beam was used as probe pulse. Prior to focusing to the sample, the probe pulse propagated through the delay line for the control of delay between the pump and probe pulses. Conversion of pump and probe pulses to 400 nm wavelength was accomplished using the 2-mm-thick barium borate (BBO) crystals. Pump and probe pulses at $\lambda = 400$ nm of similar (vertical) polarization were focused using 300-mm focal length lens on the sample contained in the 2-mm-thick fused silica cells. The pump power was 45 times higher than that of the probe beam. The zero delay between the pump and probe pulses was determined using a 0.2-mm-thick type-I BBO crystal at the focal point of two beams at the wavelength of 800 nm. Time delay between pump and probe pulses was controlled using the motorized translational stage with the single step of 7.4 μm. Ultrafast photodiode was used to measure the transmittance of the probe pulse at each position of translation stage. For the acquisition of TA profile the photodiode connected to the multi domain oscilloscope (MDO3054) and the translational stage interfaced with EPS 301 motion controller were used.

3 Results

The normalized transmittances in the case of two types of nonlinear absorption for the OA Z-scan are given by [21, 25]:

$$T(z) = 1 + \frac{I_0}{I_{sat}(x^2+1)}, \tag{1}$$

$$T(z) \approx 1 - q/2^{3/2}. \tag{2}$$

Here I_{sat} is the saturation intensity for the saturable absorption (SA), which is related with the concentration of the active centers in the medium, the effective cross-sections of involved transitions, and the lifetimes of excited states. In the case of low intensity and relatively long pulses, the SA at $\lambda = 800$ nm dominates over other NLO processes in the used samples. Other parameters are: I_0 is the intensity in the focal plane, $q = \beta I_0 L_{eff}/(1 + z^2/z_0^2)$, $z_0 = k(w_0)^2/2$ is the Rayleigh length, $k = 2\pi/\lambda$ is the wave number, w_0 is the beam waist radius at the $1/e^2$ level of intensity distribution, $L_{eff} = [1 - \exp(-\alpha_0 L)]/\alpha_0$ is the effective length of the medium, α_0 is the linear absorption coefficient, and L is the thickness of our samples ($L = 2$ mm). The linear absorption in the case of 800 and 400 nm wavelengths was measured to be 0.01 and 0.25 cm^{-1} for S1 and 0.005 and 0.15 cm^{-1} for S2 sample, respectively. Correspondingly, in the case of 800 nm probe pulses, the effective lengths of samples were almost similar to L. In the case of 400 nm pulses, this value became slightly less than L ($L_{eff} \approx 1.95$ mm for denser sample S1). Thus the absorbance of studied samples does not affect the definition of β and γ while we assume that $L_{eff} \approx L$.

CA Z-scan allows determination of nonlinear absorption and nonlinear refraction when they coexist. By defining the relative coordinate $x = z/z_0$ in general case of the joint contribution of both those processes, the normalized transmittance of samples along z-axis, $T(z)$, can be presented as:

$$T(z) = 1 + \frac{4x}{(x^2+9)(x^2+1)}\Delta\Phi_0 - \frac{2(x^2+3)}{(x^2+9)(x^2+1)}\Delta\psi_0, \tag{3}$$

where $\Delta\Phi_0 = k\gamma I_0 L_{eff}$ and $\Delta\psi_0 = \beta I_0 L_{eff}/2$ are the phase variations due to nonlinear refraction and nonlinear absorption, respectively. By making the substitution $\rho = \beta/2k\gamma$, one can get the relation between $\Delta\Phi_0$ and $\Delta\psi_0$ ($\Delta\psi_0 = \rho\Delta\Phi_0$). In that case, Eq. (3) can be re-written as follows:

$$T = 1 + \frac{2(-\rho x^2 + 2x - 3\rho)}{(x^2+9)(x^2+1)}\Delta\Phi_0. \tag{4}$$

Notice that uncertainty in determination of nonlinear absorption coefficients using the OA Z-scans was smaller compared to the CA Z-scans, thus prompting us to analyze this process using former configuration.

3.1 Determination of the NLO characteristics of Ag_2S QD suspensions

Attention was given to prevent optical breakdown of our samples. The intensities for breakdown of more dense Ag_2S suspension (S1) were measured to be 2×10^9 W cm^{-2} (for 200 ps, 400 nm pulses), 4×10^{10} W cm^{-2} (for 200 ps, 800 nm pulses), 6×10^{11} W cm^{-2} (for 60 fs, 400 nm pulses) and 8×10^{11} W cm^{-2} (for 60 fs, 800 nm pulses). Correspondingly, the maximal used intensities of probe pulses were 3×10^8 (for 200 ps, 400 nm pulses), 6×10^9 (for 200 ps, 800 nm pulses), 4×10^{11} (for 60 fs, 400 nm pulses) and 5×10^{11} W cm^{-2} (for 60 fs, 800 nm pulses). Prior to Z-scans of studies of Ag_2S suspensions, we probed the components involved in suspensions formation (TOP, butanol, methyl alcohol, and water) and found that neither of them showed noticeable nonlinear optical response at given experimental conditions.

The NLO characteristics of Ag_2S QDs were determined by analyzing the OA and CA Z-scans. The experimental records are taken by moving the sample along z-axis from negative to positive position with respect to the focal plane. Initially, the samples S1 and S2 were analyzed using picosecond pulses (Fig. 3). The S1 sample in the case of picosecond probe pulses (800 nm, 200 ps) showed SA (Fig. 3a). Notice that the SA was observed

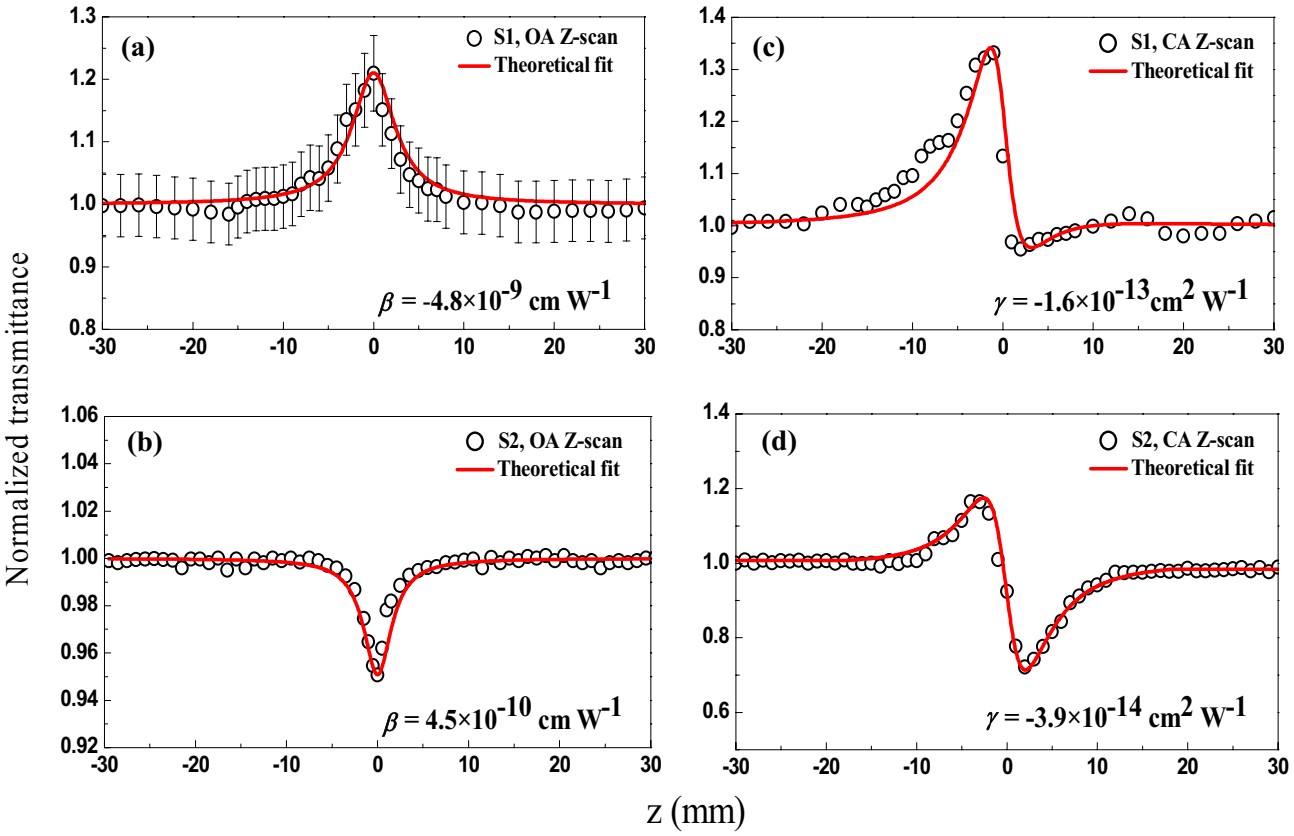

Fig. 3 OA and CA Z-scans of S1 and S2 measured using 200 ps, 800 nm probe pulses

only in the case of the high concentration of Ag_2S QDs. To fit the OA Z-scan of S1, Eqs. (1,2) were used from which we determined the I_{sat} of S1 to be 2.8×10^{10} W cm^{-2} and $\beta=-4.8\times10^{-10}$ cm W^{-1}. The fit of the OA Z-scan to the experimental data for S2 is depicted in Fig. 3b by the solid curve using Eq. (2), and the nonlinear absorption coefficient was calculated to be 4.5×10^{-10} cm W^{-1}. It was found that at small fluence (F) of 800 nm, 200 ps pulses ($F=10$ mJ cm^{-2}, $I_0=5\times10^7$ W cm^{-2}) the SA was dominating at larger concentration of QDs. This process was transformed to RSA or, most probably, 2PA at larger fluence of probe pulses ($F=50$ mJ cm^{-2}, $I_0=2.5\times10^8$ W cm^{-2}) and smaller concentration of QDs.

The error bars ($\pm5\%$) of these and other measurements of Ag_2S QD suspensions were the same during the entire course of the experiments. The example is shown in Fig. 3a. The error bars of definition of the absolute values of γ and β were estimated to be $\pm25\%$ due to uncertainty in the measurements of the intensity of laser pulses in the focal plane.

Equation (4) was used for fitting the theoretical dependences and measured normalized transmittances of CA Z-scans taking into account our experimental conditions. After fitting of ρ and $\Delta\Phi_0$ we consequently found values of γ and β for two samples. The latter parameter was close to the measurements of positive and negative nonlinear absorption performed using the OA Z-scan scheme (Fig. 3a, b).

Figure 3c, d shows the results of CA measurements demonstrating the self-defocusing in S1 and S2 samples using 800 nm, 200 ps pulses. The fitting procedure of CA Z-scans (solid curves in Fig. 3c, d) allowed to calculate γ of S1 and S2 to be -1.6×10^{-13} and -3.9×10^{-14} cm^2 W^{-1}, respectively.

In the case of shorter wavelength of the picosecond probe pulses (200 ps, 400 nm), a decrease in the normalized transmittance at focal area was observed for both samples. This process was probably related with RSA. The corresponding OA and CA Z-scans of S1 and S2 samples and their fitted curves are shown in Fig. 4. S1 showed twice larger β than S2 (Fig. 4a, b). Therefore, one can tune the nonlinear optical absorption of such suspensions by varying the concentration of Ag_2S QDs to obtain desirable applications in the UV range. Notice that, apart from concentration variations, the modification of QD's nonlinearities could be associated with their shape and size variation as well. Separate studies are necessary for clarification of this dependence. The values of β in the case of 400 nm, 200 ps probe pulses were close to the earlier reported data measured using 532-nm nanosecond pulses ($\sim5\times10^{-8}$ cm W^{-1} [32, 33]) for similar samples.

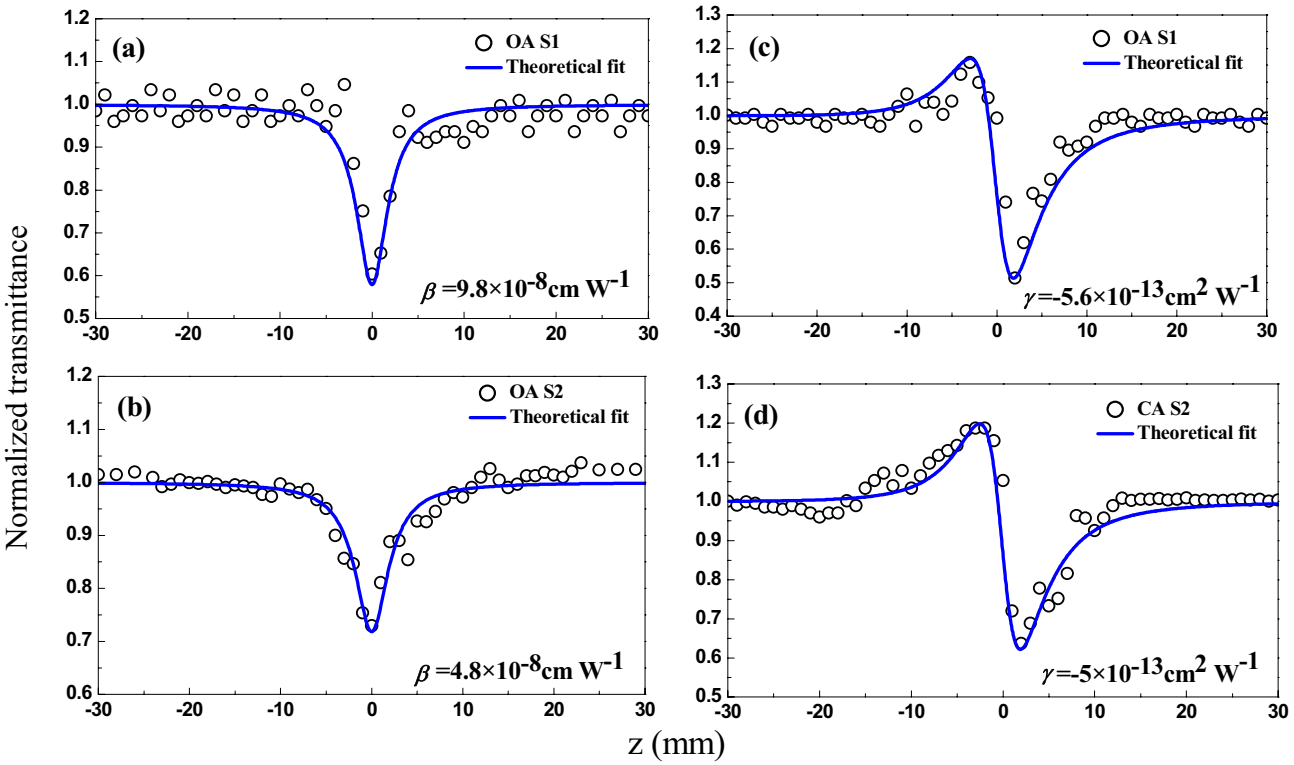

Fig. 4 OA and CA Z-scans of S1 and S2 using 200 ps, 400 nm pulses

CA measurements using 400 nm, 200 ps pulses showed self-defocusing of two samples along the whole range of probe pulse energies. γs of these two samples were nearly similar to each other (-6×10^{-13} and -5×10^{-13}cm^2 W^{-1}; Fig. 4c, d, respectively). Meanwhile, the results obtained during OA and CA Z-scans of S1 and S2 using IR femtosecond probe pulses (800 nm, 60 fs; Fig. 5c, d) were different compared to the previous case. The CA Z-scan curves showed the self-focusing, when valley was followed by the peak, contrary to the case of 400 nm, 200 ps probe pulses. The approximately similar values of γ were measured in that case (3×10^{-16} and 2.3×10^{-16} cm^2 W^{-1}). Notice that CA Z-scans using UV femtosecond pulses (400 nm, 60 fs) showed self-defocusing in sample S2, similarly to the case of 400 nm, 200 ps pulses.

SA and RSA do not play important role in Ag_2S QDs in the case of 800 nm, 60 fs pulses. For direct transition of Ag_2S QDs the excitation energy (1.55 eV) is lower than the band gap energy of Ag_2S QDs (3 eV), and, hence, the interband transition is allowed by 2PA at the laser wavelength of 800 nm. The OA Z-scans at two concentrations of Ag_2S QDs showed 2PA (Fig. 5a, b). The threefold difference in concentration of these two samples led to the decrease of the nonlinear absorption coefficient from 8.8×10^{-12} to 3.7×10^{-12} cm W^{-1}. In the case of 400 nm, 60 fs pulses, the most probable nonlinear absorption mechanism was RSA (Fig. 6, empty circles).

We also analyzed the influence of femtosecond pulse repetition rate on the OA Z-scans of S2 while significantly decreasing it from 1 kHz to 10 Hz. From these two OA Z-scan measurements we calculated the approximately similar values of β (3.7×10^{-12} and 2.9×10^{-12} cm W^{-1}). This observation suggests that the change of pulse repetition rate had no effect on the nonlinear absorption coefficient. Similar conclusion was drawn in the case of CA Z-scans using pulses of different repetition rate, which pointed out that thermal-induced self-defocusing did not play important role in the case of 1-kHz picosecond pulses. The NLO parameters of Ag_2S QD suspensions measured using 1-kHz pulses are collected in Table 1.

3.2 Pump–probe and optical limiting studies

TA in Ag_2S QDs immersed in toluene was studied using 400 nm, 60 fs pulses. We used pump pulse fluence of 20 mJ cm^{-2} ($I_0=3\times10^{11}$ W cm^{-2}) and probe pulse fluence of 0.45 mJ cm^{-2} ($I_0=7\times10^{9}$ W cm^{-2}), which fulfill the criteria for TA measurements. In Fig. 6a, we show the temporal evolution of TA. TA measurement was also performed for pure toluene to eliminate its influence on the TA profile of Ag_2S

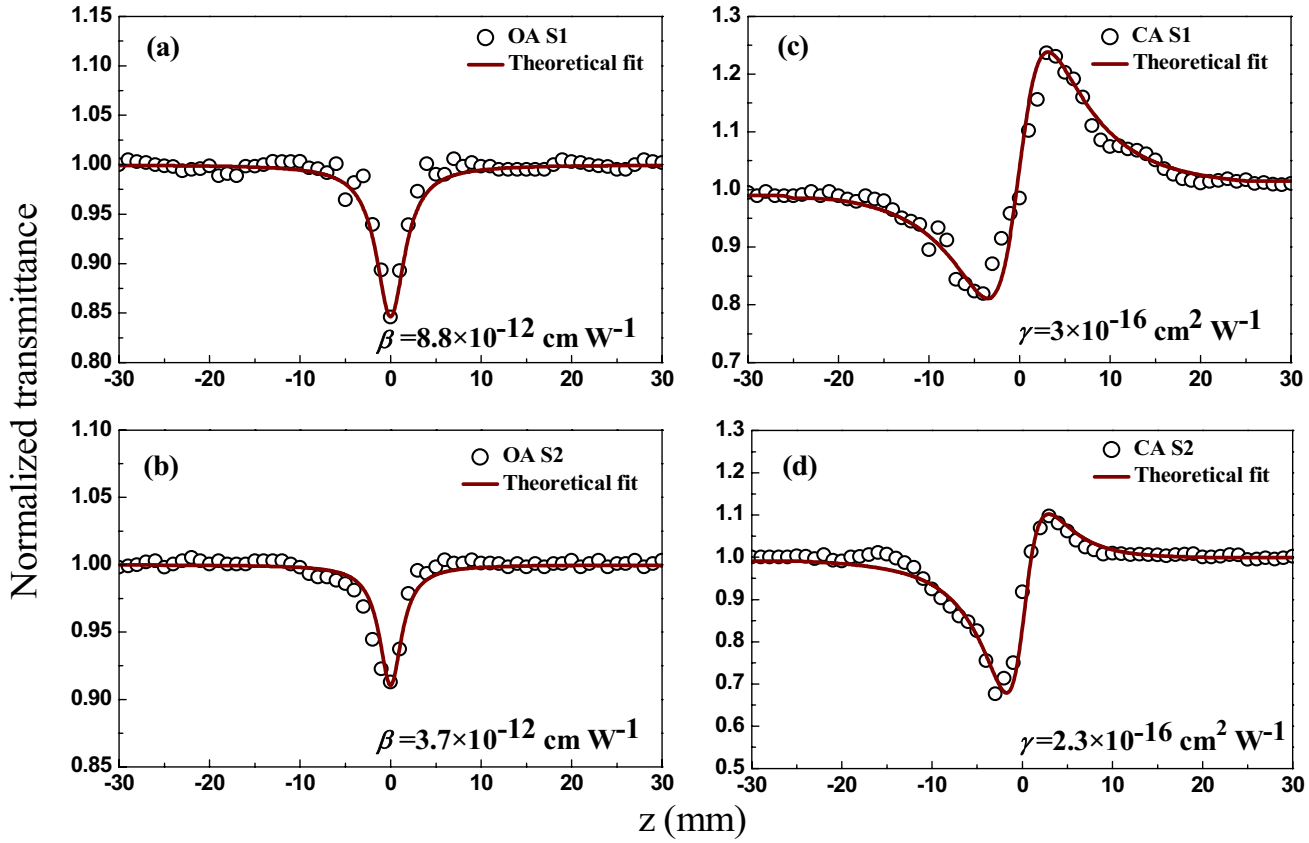

Fig. 5 OA and CA Z-scans of S1 and S2 using 60 fs, 800 nm pulses

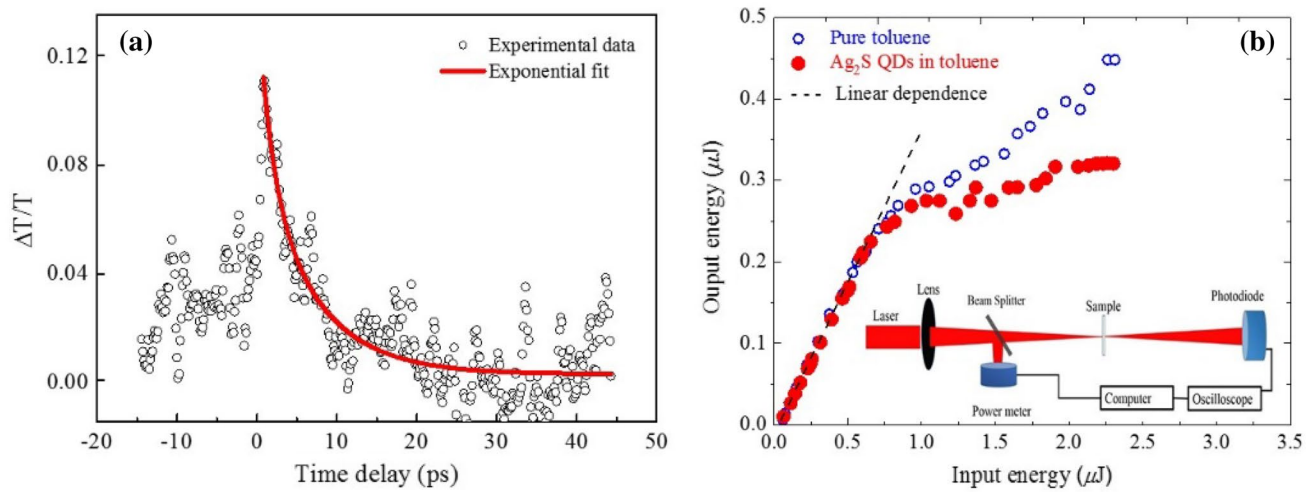

Fig. 6 **a** Transient absorption of the As_2S QDs excited at 400 nm. **b** Optical limiting of 800 nm, 60 fs pulses in pure toluene (empty circles) and Ag_2S QD suspension in toluene (filled circles). Inset: setup for optical limiting studies

QDs. TA profile was fitted with double exponential profile to obtain the decay time constants associated with relaxation of excited phonons at 400 nm irradiation. The characteristic time constants were determined to be 1.7 and 6.9 ps that can be attributed to the electron–phonon and phonon–phonon interactions in Ag_2S QDs.

Notice that there are no reports about the dynamics of the excitation of these quantum dots at resonance

Table 1 Nonlinear optical parameters of Ag_2S QD suspensions calculated at different experimental conditions

QD	I_0 (W cm^{-2})	I_{sat} (W cm^{-2})	γ (cm^2 W^{-1})	β (cm W^{-1})
Measurements using 200 ps, 800 nm radiation				
S1	3.4×10^{8}	2.8×10^{10}	-1.6×10^{-13}	-4.8×10^{-9}
S2	1.8×10^{9}		-3.9×10^{-14}	4.5×10^{-10}
Measurements using 200 ps, 400 nm radiation				
S1	8.9×10^{7}		-5.6×10^{-13}	9.8×10^{-8}
S2	8.9×10^{7}		-5×10^{-13}	4.8×10^{-8}
Measurements using 60 fs, 800 nm radiation				
S1	2.2×10^{11}		3×10^{-16}	8.8×10^{-12}
S2	2.7×10^{11}		2.3×10^{-16}	3.7×10^{-12}
Measurements using 60 fs, 400 nm radiation				
S2	1×10^{11}		-2×10^{-15}	5×10^{-11}

conditions. The determined time constants are consistent with the earlier reported data [34, 35] where TA studies were performed for the case of Ag_2S QDs in ethylene glycol in the near-IR region. The relaxation dynamics, which can become faster as the pump pulse energy increases, was attributed to Auger recombination process. However, in our experiments the SPR at ~ 400 nm corresponded to the quasi-resonant conditions for the Ag_2S QDs irradiated by 400 nm pulses. This can probably lead to saturation of absorbance followed with the increase in the transmittance of probe pulses at higher intensity of pump radiation at the employed concentration (S1) of Ag_2S QDs in toluene.

The OL was demonstrated using the 800 nm, 60 fs pulses propagating through the Ag_2S QD suspension in toluene. This effect was attributed to 2PA. The suspension was placed close to the focal plane of 400 mm focal length lens (see inset in Fig. 6b). The energy of 800 nm pulses was gradually increased and measured before and after propagation through the 2-mm-thick cell containing QD suspension S2 (Fig. 6b, filled circles). The linear dependence between input and output pulses was maintained up to the input pulse energy of ~ 0.7 μJ. The transmittance of QD-containing cell decreased with further growth of pulse energy. This decrease of transmittance with the growth of laser intensity was also observed in the OA Z-scan measurements using 800 nm, 60 fs pulses (Fig. 5a, b). Further increase of input pulse energy led to OL of the energy of propagated laser radiation. OL was also observed in the case of pure toluene starting from approximately the same energy (0.8 μJ; Fig. 6b, empty circles). These two curves show that QDs enhance the OL of this suspension even compared to the liquid (toluene) possessing large nonlinear absorption.

4 Discussion

Previously, analysis of the sign variations of γ was performed in the case of semiconductors [36]. The used Kramers–Kronig model provided some clues in definition of γ's sign transformation from self-focusing to self-defocusing and vice versa once one uses different wavelengths of probe pulses. The crucial parameter in their model is the band gap value of semiconductor. Meanwhile, once the sizes of semiconductor decrease below ~ 5–10 nm their band gap drastically increases. It is not clear whether it is correct to consider Ag_2S QDs as semiconductors. Below we address the modification of the sign of nonlinear refractive index using the Kramers–Kronig relations for QDs.

An important characteristic of metal sulfide QDs is the band gap controllable by the size effect. This peculiarity of QDs can strongly change their NLO properties, in particular the sign of nonlinear refraction. The analysis of nonlinear refraction of S1 and S2 showed that they demonstrate self-focusing properties (Fig. 5a, b) once femtosecond 800 nm pulses were used as the probe radiation. The nonlinear Kramers–Kronig relations predict the self-focusing in semiconductors for which the relation $\hbar\omega/E_g < 0.69$ takes place [36]. Here $\hbar$ is the Planck's constant, ω is the frequency of laser radiation, and E_g is the bandgap energy of semiconductor (3 eV in the case of Ag_2S QDs). The corresponding $\hbar\omega/E_g$ value for suspensions at $\lambda = 800$ nm was calculated to be 0.53. Thus, one can expect a positive sign of γ in these two suspensions (S1 and S2) that was confirmed in our experiments. Correspondingly, the experiments with 400 nm, 60 fs probe pulses showed the self-defocusing properties of our samples that corroborates with above consideration ($\hbar\omega/E_g = 1.06$). The reason of relatively small values of nonlinear refractive indices of the Ag_2S QD suspensions at 800 nm (3×10^{-16} cm^2 W^{-1}) can be related with the proximity of their $\hbar\omega/E_g$ values to 0.69 (i.e., at $\lambda \approx 620$ nm) where the sign of γ changed from positive to negative. Far from this wavelength (i.e., at 400 nm) the nonlinear refractive index showed notably larger value (2×10^{-15} cm^2 W^{-1}).

Meanwhile, the use of longer probe pulses demonstrated the self-defocusing properties of the studied samples in the case of both 400 and 800 nm radiation (Figs. 3, 4). Below we analyze the change of sign of nonlinear refraction in the case of longer pulses. There are some fast processes (intermolecular interaction, molecular reorientational Kerr effect, electronic Kerr effect) that can originate from the nonlinear optical response of Ag_2S particles and contribute to the overall nonlinear adding of the refractive index. The slowest among them is the process connected with the reorientation of molecules. Previously, the relaxation times of these three processes were reported as ~ 1.5 ps

for reorientation of molecules [37] and ~200 fs for other processes [38]. The former process can either increase the effective nonlinear refractive index (in the case of positive value of reorientational processes [39]) or decrease or even change the sign of this parameter in the case of relatively long pulses. Our results indicating the change of the sign of γ at a probe pulse duration (200 ps) compared to the 60 fs pulses confirm the assumption of the negative addition of some nonlinearities (intermolecular interaction and molecular reorientational Kerr effect) to the purely electronic Kerr effect attributed to the influence of ultrafast pulses. In other words, the growth of pulse duration above the femtosecond range can lead to involvement of the above-mentioned slow processes, which overpassed the purely electronic Kerr effect in our samples. The negative value of the former processes causes the change of sign of the effective nonlinear refractive index of suspension.

Notice that actual values of the nonlinear susceptibilities of QDs are considerably higher than those of QD suspensions due to small fraction of particles in the whole volume of solvent. A simplest method for the estimation of the nonlinear susceptibilities of such particles is to divide the nonlinear susceptibility of compound by the volume or weight part of QDs. More precisely, the third-order nonlinear susceptibilities [$\chi^{(3)}$] of composites, and, correspondingly, γ and β, are also enhanced by the local field factor as

$$\chi^{(3)} = p|f|^2 f^2 \chi^{(3)}_{QD}, \tag{5}$$

where $\chi^{(3)}{}_{QD}$ is the third-order nonlinear susceptibility of QDs, f is the local field factor, which in the case of Ag_2S QDs was analyzed in Refs. [40, 41], and p is the volume fraction of nanoparticles or QDs. The square of the local field factor for the semiconductor QDs embedded in many dielectric materials is often of the order of 0.2–0.4 [40].

The NLO parameters shown in Table 1 are attributed to the suspensions of Ag_2S QDs. Our estimates show that the volume fraction of QDs in suspensions was in the range of 10^{-3}. In particular, β of S1 suspension at 400 nm, 200 ps probe pulses was measured to be ~ 10^{-7} cm W^{-1}. One can estimate β of QDs at these conditions to be ~ 1×10^{-3} cm W^{-1} taking into account the volume fraction of small-sized species in the solution and local field factor ($|f|^2 \sim 0.3$). Similarly, each value of γ and β of suspensions presented in Table 1 should be divided by a factor of $p|f|^2 f^2 \approx 10^{-4}$ to determine these parameters attributed to Ag_2S QDs.

In these studies, we used the aqueous suspensions of Ag_2S quantum dots. To explain the increase in the nonlinear optical response of this suspension, we considered the local field factor. Meanwhile, the medium in which the studies were conducted is a composite material. Therefore, it is worth additionally analyzing it as an "effective" medium consisting of two components possessing different nonlinearities.

Actually, the suspensions consisted on the water and QDs, while the concentration of some other residual components participated in the synthesis of quantum dots was notably smaller with regard to the two main species. We checked the nonlinear optical response of water at used experimental conditions. Neither fast (i.e., Kerr-related) nonlinear optical properties nor slow thermal accumulation-induced effects were observed in water at the maximal used intensities and energies of 200 ps and 60 fs pulses. Particularly, our studies showed the insignificant role of thermal-induced variations of the refractive indices of suspensions at 1 kHz pulse repetition rate. Thus the surrounding medium did not play role of thermal lens or Kerr medium along the whole set of these studies. From this we concluded that the NLO processes observed during these studies can be attributed solely to the presence of Ag_2S QDs in the suspensions.

Our measurements allowed determination of the relative role of nonlinear absorption and nonlinear refraction in Ag_2S QDs. The Stegeman figure of merit $T = |2\beta\lambda/\gamma|$ shows the prevailing influence of nonlinear absorptive properties of used QDs over their nonlinear refraction ($T = 5$ and $T = 4.8$ in case of picosecond and femtosecond pulses at both 800 and 400 nm, respectively).

Below we briefly address the usefulness of analysis and variations of the NLO parameters in small-sized QDs with respect to larger-sized nanoparticles. The QDs with sizes less than 4 nm can play a predominant role in the overall nonlinear refractive index of such structures due to the quantum confinement effect. The positive sign of γ attributed to small QDs can prevail with respect to the negative sign of γ in the case of larger-sized nanoparticles when electronic Kerr effect plays dominating role in the NLO variations of refractive index. This peculiarity can lead to the difference in the NLO properties of bulk materials, large-sized nanoparticles, and small-sized QDs. Moreover, as our studies show, pulse duration is another dominating factor for determination of the sign of γ of these species.

5 Conclusions

In conclusion, we have analyzed the NLO properties of 4-nm Ag_2S QD suspensions using 60-fs and 200-ps pulses of 800-nm and 400-nm radiation. At 400 nm, 200 ps pump pulses, those QDs have demonstrated large nonlinear absorption (up to $\beta \approx 10^{-3}$ cm W^{-1}) comparable with the highest reported values using nanosecond laser irradiation at 532 nm, and relatively strong nonlinear refraction ($\gamma = -6 \times 10^{-9}$ cm^2 W^{-1}). The relatively high nonlinear absorption coefficients of QDs (up to 8.8×10^{-8} cm W^{-1}) and moderate nonlinear refractive indices (up to 3×10^{-12} cm^2 W^{-1}) were obtained using 800 nm, 60 fs pump. We have shown that the nonlinear absorption of Ag_2S QDs can be more effectively used

for optical limiting of femtosecond pulses compared to the toluene, which has large nonlinear absorption. The analysis of transient absorption of QDs allowed determination of the time constants attributed to electron–phonon (1.7 ps) and phonon–phonon (6.9 ps) processes.

We systematically analyzed the dynamics of variations of the sign of nonlinear refraction at different pulse widths and wavelengths of probe radiation. Overall, our studies of nonlinear absorption and refraction of Ag_2S QDs may allow definition of the optimal conditions of excitation of these QDs for high-order harmonic generation during formation of plasma plumes containing such species. The large RSA may indirectly indicate the possibility of some transitions to be involved in the growth of nonlinear susceptibility and the enhancement of single harmonic or group of harmonics during frequency conversion of ultrashort laser pulses interacting with such QDs.

Acknowledgements R.A.G. thanks the financial support from Chinese Academy of Sciences President's International Fellowship Initiative (Grant no. 2018VSA0001).

Funding National Natural Science Foundation of China (Grant nos. 91750205, 61774155); National Key Research and Development Program of China (2017YFB1104700).

References

1. P. Işık, A. Karatay, H. Gul Yaglioglu, A. Elmali, U. Kürüm, A. Ateş, N. Gasanly, Opt. Commun. **288**, 107 (2013)
2. I.L. Bolotin, D.J. Asunskis, A.M. Jawaid, Y. Liu, P.T. Snee, L. Hanley, J. Phys. Chem. C **114**, 16257 (2010)
3. Q. Li, C. Liu, L. Zang, Q. Gong, X. Yu, C. Cao, J. Opt. Soc. Am. B **25**, 1978 (2008)
4. X. Liu, Y. Adachi, Y. Tomita, J. Oshima, T. Nakashima, T. Kawai, Opt. Express **20**, 13457 (2012)
5. I. Gur, N.A. Fromer, M.L. Geier, A.P. Alivisatos, Science **310**, 462 (2005)
6. V.L. Colvin, M.C. Schlamp, A.P. Allvisatos, Nature **370**, 354 (1994)
7. S. Abe, J.J. Joos, L.I.D.J. Martin, Z. Hens, P.F. Smet, Light Sci. Appl. **6**, e16271 (2017)
8. V.M.N. Tessler, M. Kazes, S. Kan, U. Banin, Science **295**, 3 (2002)
9. D.L. Klein, R. Roth, A.K.L. Lim, A.P. Alivisatos, P.L. McEuen, Nature **389**, 3 (1997)
10. D.V. Talapin, C.B. Murray, Science **310**, 86 (2005)
11. Z. Zhang, Z. You, D. Chu, Light Sci. Appl. **3**, e213 (2014)
12. W.C. Chan, S. Nie, Science **281**, 2016 (1998)
13. M. Bruches Jr., M. Moronne, P. Gin, S. Weiss, A.P. Alivisatos, Science **281**, 2013 (1998)
14. R.A. Ganeev, A.I. Ryasnyansky, T. Usmannov, Opt. Quantum Electron. **35**, 211 (2003)
15. G.S. Boltaev, B. Sobirov, S. Reyimbaev, H. Sherniyozov, T. Usmanov, M.S. Smirnov, O.V. Ovchinnikov, I.G. Grevtseva, T.S. Kondratenko, H.S. Shihaliev, R.A. Ganeev, Appl. Phys. A **122**, 999 (2016)
16. L.W. Liu, S.Y. Hu, Y.P. Dou, T.H. Liu, J.Q. Lin, Y. Wang, Beilstein J. Nanotechnol. **6**, 1781 (2015)
17. P. Kumbhakar, M. Chattopadhyay, A.K. Mitra, Int. J. Nanosci. **10**, 177 (2011)
18. Z. Zeng, C.S. Garoufalis, A.F. Terzis, S. Baskoutas, J. Appl. Phys. **114**, 023510 (2013)
19. H. Linnenbank, Y. Grynko, J. Förstner, S. Linden, Light Sci. Appl. **5**, e16013 (2016)
20. L. Gao, C. Chen, K. Zeng, C. Ge, D. Yang, H. Song, J. Tang, Light Sci. Appl. **5**, e16126 (2016)
21. O.V. Ovchinnikov, M.S. Smirnov, A.S. Perepelitsa, T.S. Shatskikh, B.I. Shapiro, Quantum Electron. **45**, 1143 (2015)
22. Y.P. Sun, J.E. Riggs, K.B. Henbest, R.B. Martin, J. Opt. Soc. Am. B **9**, 481 (2000)
23. R.B. Matin, M.J. Meziani, P. Pathak, J.E. Riggs, D.E. Cook, S. Perera, Y.-P. Sun, Opt. Mater. **29**, 788 (2007)
24. R. Karimzadeh, H. Aleali, N. Mansour, Opt. Commun. **284**, 2370 (2011)
25. M. Sheik-Bahae, A.A. Said, T.H. Wei, D.J. Hagan, E.W. Van Stryland, IEEE J. Quantum Electron. **26**, 760 (1990)
26. G. Fan, S. Qu, Q. Wang, C. Zhao, L. Zhang, Z. Li, J. Appl. Phys. **109**, 023102 (2011)
27. H. Zeng, Y. Yang, X. Jiang, G. Chen, J. Qiu, F. Gan, J. Cryst. Growth **280**, 516 (2005)
28. R.A. Ganeev, G.S. Boltaev, R.I. Tugushev, T. Usmanov, Appl. Phys. B **100**, 571 (2010)
29. R.A. Ganeev, A.I. Ryasnyansky, A.T. Stepanov, T. Usmanov, Opt. Quantum Electron. **36**, 949 (2004)
30. R.A. Ganeev, M. Suzuki, M. Baba, M. Ichihara, H. Kuroda, J. Appl. Phys. **103**, 063102 (2008)
31. A. Sahu, L. Qi, M.S. Kang, D. Deng, D.J. Norris, J. Am. Chem. Soc. **133**, 6509 (2011)
32. H. Aleali, N. Mansour, M. Mirzaie, Eng. Technol. Int. J. Phys. Math. Sci. **8**, 1274 (2014)
33. H. Aleali, N. Mansour, Optik **127**, 2485 (2016)
34. W.J. Mir, A. Swarnkar, R. Sharma, A. Katti, K.V. Adarsh, A. Nag, J. Phys. Chem. Lett. **6**, 3915 (2015)
35. J. Sun, W. Yu, A. Usman, T.T. Isimjan, S. Dgobbo, E. Alarousu, K. Takanabe, O.F. Mohammed, J. Phys. Chem. Lett. **5**, 659–665 (2014)
36. M. Sheik-Bahae, D. Hutchings, D.J. Hagan, E.W. Van Stryland, IEEE J. Quantum Electron. **27**, 1296–1309 (1991)
37. J. Etchepare, G. Grillon, J.P. Chambaret, G. Hamoniaux, A. Orszag, Opt. Commun. **63**, 329–335 (1987)
38. T. Kawazoe, H. Kawaguchi, J. Inoue, O. Haba, M. Ueda, Opt. Commun. **160**, 125 (1999)
39. R.A. Ganeev, A.I. Ryasnyansky, M. Baba, M. Suzuki, N. Ishizawa, M. Turu, S. Sakakibara, H. Kuroda, Appl. Phys. B **78**, 433 (2004)
40. L. Jing, S.V. Kershaw, Y. Li, X. Huang, Y. Li, A.L. Rogach, M. Gao, Chem. Rev. **116**, 10623 (2016)
41. F. Nan, F.-M. Xie, S. Liang, L. Ma, D.-J. Yang, X.-L. Liu, J.-H. Wang, Z.-Q. Cheng, X.-F. Yu, L. Zhou, Q.-Q. Wang, J. Zeng, Nanoscale **8**, 11969 (2016)